

Dissipation Mechanisms in Thermomechanically Driven Silicon Nitride Nanostrings

A. Suhel,¹ B. D. Hauer,¹ T. S. Biswas,¹ K. S. D. Beach,^{1,*} and J. P. Davis^{1,2,†}

¹*Department of Physics, University of Alberta,
Edmonton, Alberta, Canada T6G 2E9*

²*Canadian Institute for Advanced Research: Nanoelectronics
Program, Toronto, Ontario, Canada M5G 1Z8*

(Dated: Version January 10, 2012)

Abstract

High-stress silicon nitride nanostrings are a promising system for mechanical sensing applications because of their ultra-low mechanical dissipation, despite their relatively small mass. By performing thermomechanical calibration across multiple vibrational modes, we are able to assess the roles of the various dissipation mechanisms in these devices. Specifically, we possess a set of nanostrings in which all measured modes fall upon a single curve of peak displacement versus frequency, even while their mechanical Q s vary. This allows us to rule out bending and intrinsic loss mechanisms as dominant sources of dissipation and to conclude that the most significant dissipation mechanism in high-stress nanostrings is clamping loss.

* kbeach@ualberta.ca

† jdavis@ualberta.ca

The extremely high values of mechanical Q that have been reported in silicon nitride nanostrings [1–3] have generated a great deal of excitement in the nanomechanics community [4]. These devices seem to be ideal for use in mass sensing [5], temperature sensing [6], optomechanics [7–9], and research into the quantum properties of nanoscale resonators [10]. Nanostrings possess all the desired properties for these endeavors, including small mass, high frequency, and high Q , with correspondingly large displacement amplitudes. This combination makes them sensitive to external perturbation, such as the addition of adsorbed mass, while remaining within the limits of current detection techniques [11]. In this manuscript we demonstrate thermomechanically limited detection of up to six mechanical modes of nanostrings, allowing us to accurately calibrate all these modes. Furthermore, we present a set of devices in which all harmonics fall upon a single curve of calibrated peak displacement versus frequency. As we discuss below, this allows us to conclude that the mechanical Q is limited by clamping at the boundaries (the leakage of phonons from the nanostring through the clamping points), suggesting a method to further engineer the mechanical Q .

It has been argued that the large mechanical Q in silicon nitride nanostrings stems from the fact that the devices are under extremely high tensile stress ($\sigma = 0.8$ GPa for our devices), causing tension along the length of a nanostring, and the stored elastic energy from tension increases the Q [3]. The source of dissipation in these devices is intriguing since it is overall significantly lower than in similar non-stressed systems of the same dimensions. Experiments have shown an increasing Q with mechanical tensioning of non-prestressed (low tension, non-stoichiometric silicon nitride) devices [12, 13], corroborating the role of the tension in the Q .

In addition to the high Q , the tension compels the devices to behave as strings instead of the traditional doubly clamped beams one would expect for this geometry. The harmonics are at integer multiples of the fundamental frequency [14], $\nu_n = n\nu_1$, where ν_1 is the fundamental mode frequency and n indicates the mode number. And the mode frequency depends only on the length of the string (and not on the width or thickness). These features are in contrast to the more complicated harmonics of doubly clamped beams [15], which are demonstrated by low-stress silicon nitride devices of the same geometry [16]. Furthermore, it has now been shown that very high mechanical Q s exist for nanostrings under tension in a variety of other materials, including the polymer SU-8 [17], aluminum [6, 18], and AuPd [19], strongly suggesting that the high Q is a product of the tension and string-like behavior, and not a special property of silicon nitride itself.

There is a significant potential of nanostrings for sensing applications [20], and likely many

materials can be made to have high Q , and therefore become significantly better sensors, if they can withstand high tensile stress. An important factor in sensing applications is accurate calibration [21]. This can be performed via thermomechanical calibration, which allows determination of the absolute displacement of the nanostrings [22], although the procedure is often restricted to the fundamental mode since it has the largest displacement. Because of the high Q of nanostrings, we are able to detect the thermomechanical motion of up to six harmonics for our longest strings. A key insight is that such multimode thermomechanical calibration can reveal important information about the dissipation mechanisms in nanostrings.

Our silicon nitride nanostrings are fabricated from stoichiometric silicon nitride deposited onto silicon dioxide on a silicon handle using LPCVD. This is quite cost effective as wafers are commercially available for \approx \$50 for a 100 mm wafer (Rogue Valley Microdevices). We pattern photoresist spun onto the wafer using standard optical lithography. The wafers are diced into chips, the pattern in the developed photoresist is transferred to the silicon nitride using reactive ion etching, and the photoresist is subsequently removed. The nanostrings are released from the substrate by etching the 2 μm thick silicon dioxide layer using buffered oxide etch.

The completed devices, shown in Figs. 1(h) and 1(i), are mounted onto a piezoelectric, which

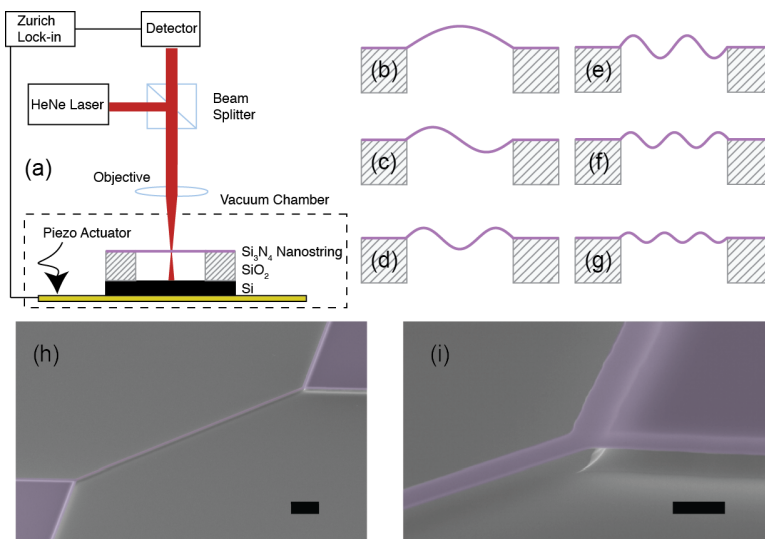


FIG. 1. (a) Schematic of our measurement set-up. The silicon nitride nanostring is mounted in an optical access vacuum chamber. (b–g) Cartoons showing the mode shapes of the first six harmonics of a nanostring. (h–i) Scanning electron micrographs of the 215 μm long silicon nitride nanostring, with scale bars of length 20 μm and 3 μm respectively.

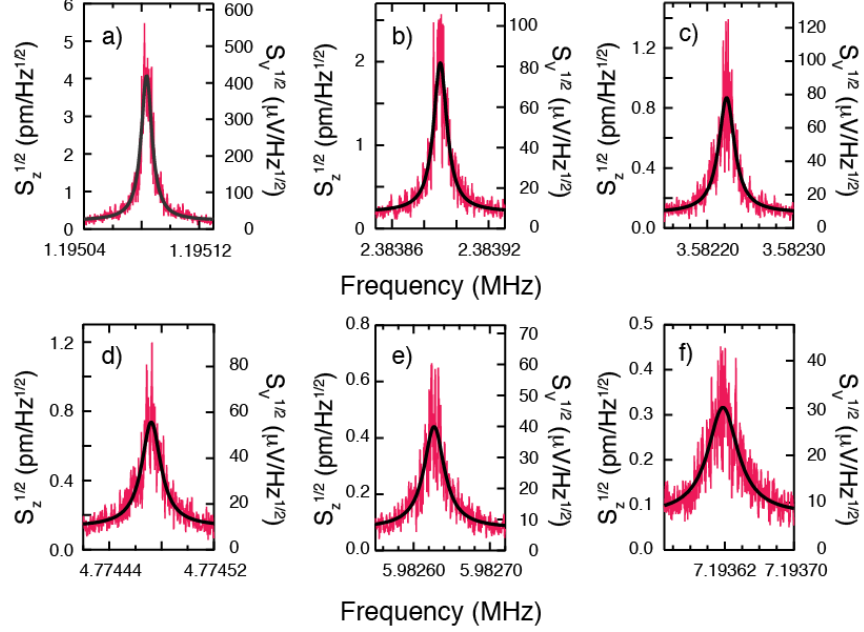


FIG. 2. Calibrated thermomechanical spectra of the first six harmonics of the 215 μm long nanostring, with fits to the data using the power spectral density function [23]. These are single sweeps and are post-processed by a sliding average over five points.

can provide mechanical actuation when excited by the lock-in amplifier (Zurich Instruments HF2LI). The sample and piezoelectric are mounted into a short-working-distance vacuum chamber that is maintained at a pressure of $\approx 2 \times 10^{-6}$ torr. This is sufficiently low to eliminate pressure related damping [13]. The out-of-plane displacement of the nanostring is measured via optical interference with respect to the silicon substrate (HeNe 632.8 nm focused to an $\sim 1 \mu\text{m}$ diameter spot with a long working length objective), as shown in Fig. 1(a) [24]. Interferometric detection can be performed with or without a voltage applied to the piezo. In the latter case—appropriate for measurement of the thermomechanical actuation—the Zurich lock-in amplifier acts as a spectrum analyzer with a user controlled measurement bandwidth. Because the Q s of the devices are high, a bandwidth of only 1 Hz is required. This bandwidth is identified by verifying that the Q measured via thermomechanical actuation is consistent with the driven Q , as well as with a ringdown measurement versus time.

In a simple model, the string is described by its vertical displacement $z(x, t)$, which is a function of the horizontal position x along the string and the time t . The string endpoints are fixed at $z(0, t) = z(L, t) = 0$, and the string achieves its natural length L when the displacement of the string is everywhere zero. In the linear regime—applicable for all measurements reported here—

the length of the string deviates from L by an amount $\int_0^L dx z_x^2$. (Here $z_x = \partial z(x, t)/\partial x$ denotes the partial derivative.) By virtue of the strong intrinsic tensile stress σ of the silicon nitride, there is a corresponding restoring force proportional to the local curvature when the string is stretched. Hence, the string obeys a modified wave equation $\rho z_{tt} = \sigma z_{xx} - D[z(x, t)]$, where the functional D encodes the various dissipative processes in operation.

It is convenient to decompose the motion of the system into its normal modes

$$z(x, t) = \sum_n a_n(t) \sin\left(\frac{n\pi x}{L}\right), \quad (1)$$

which are indexed by a positive integer n , the mode number. The first six mode shapes are sketched in Fig. 1(b)–(g). Each mode acts as a nearly independent damped harmonic oscillator obeying

$$m \frac{d^2 a_n}{dt^2} + \gamma_n \frac{\partial a_n}{\partial t} + m \omega_n^2 a_n = f_n(t). \quad (2)$$

Here, m is the geometric mass of the string, ω_n the angular frequency, and γ_n the damping coefficient ($\gamma_n = m\omega_n/Q_n$). In the case of thermomechanical actuation, the forcing term $f_n(t)$ can be understood as a continuous-time stochastic process that acts as a source of thermal noise. The sequence of resonance frequencies

$$\nu_n = \frac{\omega_n}{2\pi} = \frac{n}{2L} \sqrt{\frac{\sigma}{\rho}} \quad (3)$$

depends on the device length and on the intrinsic tensile stress and density ρ of the silicon nitride [8]. Values in the literature for the density vary, and therefore we use our measured frequencies and lengths, along with the tensile stress reported by the manufacturer, $\sigma = 0.8$ GPa, to determine the density to be 3000 kg/m^3 , consistent with other reported values [25].

We now briefly discuss the form of the damping coefficient. Since the experimental chamber is evacuated to $\approx 2 \times 10^{-6}$ torr, the dissipation cannot have a substantial contribution from any viscous term z_t that depends on the absolute motion of the string [13]. Instead, the leading order contribution from internal material processes must go as $z_{xx,t}$, which describes how fast a volume element in the string is moving with respect to neighboring ones. The exception is in the vicinity of the end points, where dissipation can depend on the time rate of change of the angle that the string makes with respect to its connection point ($z_{x,t}$). By this reasoning, the effective Q for each mode is well approximated by

$$Q_n = \frac{m\omega_n}{\gamma_n} \approx \frac{m}{\tilde{\gamma}^{\text{visc}}\omega_n^{-1} + \tilde{\gamma}^{\text{clamp}} + \tilde{\gamma}^{\text{bend}}\omega_n}.$$

Here, we have taken γ_n to be a sum of three contributions $\gamma_n^{\text{visc}} = \tilde{\gamma}^{\text{visc}} \approx 0$, $\gamma_n^{\text{clamp}} = \tilde{\gamma}^{\text{clamp}} \omega_n \sim \sigma^{-1/2} \omega_n$, and $\gamma_n^{\text{bend}} = \tilde{\gamma}^{\text{bend}} \omega_n \sim (1/\sigma) \omega_n^2$ that are meant to describe viscous damping, clamping losses, and bending losses, respectively.

Note that there is a characteristic mode number dependence to each contribution. In particular, Q values that are constant across modes are indicative of dissipation dominated by clamping loss. This is consistent with our understanding that the relative contribution $\tilde{\gamma}^{\text{bend}}/\tilde{\gamma}^{\text{clamp}} \sim 1/\sqrt{\sigma}$ is likely to be small in high stress materials.

Thermomechanical calibration allows us to quantitatively compare these loss mechanisms. Once a thermally driven spectrum is acquired, as in Fig. 2, we calibrate the voltage signal to an absolute displacement via the equipartition theorem. Fitting the power spectral density function [23] to the square of the voltage signal divided by the measurement bandwidth, we extract four parameters: the displacement noise floor, the Q , the resonance frequency, and the conversion factor between the voltage signal and the displacement, α (with units m^2/V^2). The only uncertainty is the mass of the nanostring, which we compute as $m = \rho L w t$. The thickness $t = 250$ nm is the same in all devices, whereas the width w is idiosyncratic. Therefore accurate knowledge of the density and geometry is important for this calibration. The main results are the peak displacement of the beam at the resonance frequency (Fig. 3a), and the quality factor Q_n (Fig. 3b), both of which are extracted from the fit to the calibrated spectrum. Calibration is repeated for each measurement of a resonance spectrum, since α varies with the location of our laser spot.

The peak displacements and frequencies of the second mode of the 215 μm device and the first mode of the 102 μm device are nearly identical [see Fig. 3(a)]. The coincidence of the frequencies (following from the near identity $1/102 \approx 2/215$) is a consequence of the n/L scaling in Eq. (3). As is characteristic of strings, the frequency is proportional to the sound velocity and mode number but otherwise depends only on the string length and not on any of its transverse dimensions. There are additional degeneracies—the 3rd mode of the 215 μm device and the 1st mode of the 74 μm device; the 4th mode of the 215 μm device and the 2nd of the 102 μm device; the 6th mode of the 215 μm device, the 3rd of the 102 μm device, and the 2nd of the 74 μm device—that together constitute proof of these systems’ string-like behavior.

On the other hand, it is not obvious that modes with identical frequencies should also have identical peak displacements, as seen in Fig. 3(a). This behavior of the peak displacement is not universal. Rather, it is simply fortuitous that we have three devices that fall on the same curve, and we have measured other devices that do not fit this trend (for example devices measured at higher

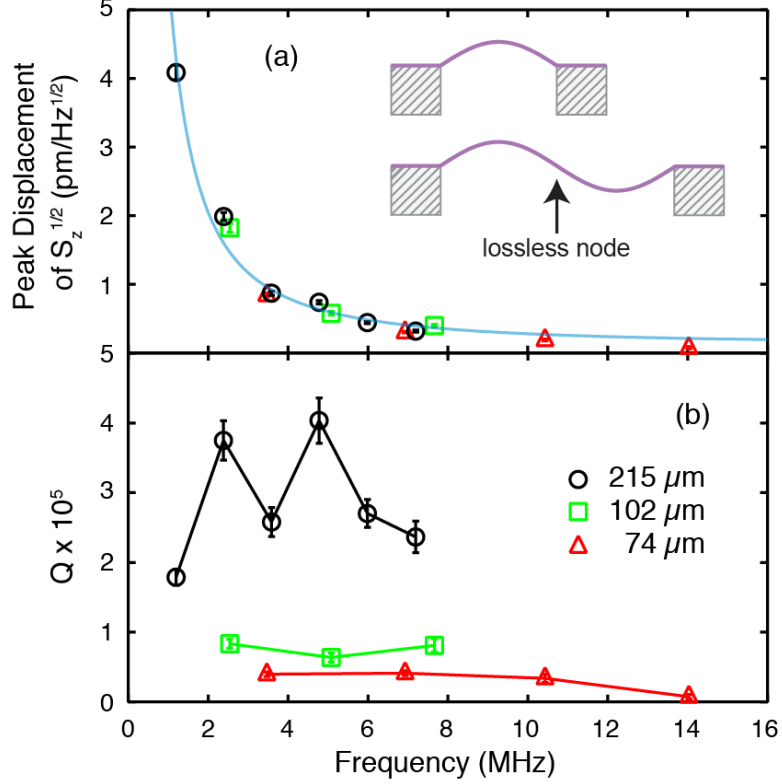


FIG. 3. (a) Peak displacement and (b) Q from thermomechanical calibration of three devices, all 250 nm thick. Black circles are for a string 215 μm long and 2.1 μm wide, green squares for 102 μm long and 1.1 μm wide, red triangles for 74 μm long and 1.2 μm wide. The blue curve in (a) is a fit to Eq. 5.

pressures). The fact that these devices were manufactured identically, from the same wafer, and measured under rigorously controlled conditions, aids in the coincidence.

In Fig. 3(b), the harmonics of a longer device are seen to have higher Q (lower dissipation) than the modes of a shorter device with identical frequencies. Conveniently, there exist in our data set modes from different devices that have identical peak displacements but substantially different Q s. We must conclude that the two modes differ only in clamping loss. Specifically, since they have identical peak displacements, these modes have identical local curvature, and therefore the Q cannot be limited by dissipation due to bending [26]. Since the materials and fabrication are identical, the only difference between such modes is the ratio of clamping points (two) to the number of lossless nodes ($n - 1$) [see inset to Fig. 3(a)]. The smaller this ratio, the smaller the effective clamping.

Moreover, our analytical results tell us that the peak displacement versus frequency curve contains quantitative information about the dissipation mechanisms [23]. In particular, if it is true that

clamping loss dominates, then the peak displacement should decay like $1/\nu_n^{3/2}$. A more precise statement of the predicted frequency dependence is as follows: the spectral density of the squared displacement is

$$S_n(\nu_n^{\max}) = \frac{Q_n k_B T}{m\pi^3(1 - \frac{1}{4Q_n^2})\nu_n^3}; \quad (4)$$

the corresponding displacement $\Delta z = \sqrt{S_n(\nu_n^{\max})\Delta\nu}$ for an arbitrary frequency interval $\Delta\nu$ goes like

$$\begin{aligned} \sqrt{\frac{Q_n}{\nu_n^3}} &\sim \frac{1}{\nu_n^{3/2} \sqrt{\tilde{\gamma}^{\text{clamp}}} \sqrt{1 + (\tilde{\gamma}^{\text{bend}}/\tilde{\gamma}^{\text{clamp}})2\pi\nu_n}} \\ &\sim \frac{1}{\nu_n^{3/2} + \tau\nu_n^{5/2}}. \end{aligned} \quad (5)$$

The fit shown in Fig. 3(a) is of this form and achieved with a value $\tau = \pi\tilde{\gamma}^{\text{bend}}/\tilde{\gamma}^{\text{clamp}} = (-0.3 \pm 2.5) \times 10^{-7}$ s that is effectively zero within measurement error. The limit $\tau^{-1} \gg \nu_1$ implies that the ratio of bending to clamping loss is negligible.

Identification of clamping as the major source of dissipation provides a path for further increasing the Q of nanostrings under tensile stress. Specifically, one could design clamping points at the ends of the beams that either carefully suspend the device [27], or reflect phonons back into the string instead of allowing them to leak into the substrate. This has been achieved in part in Ref. 3 by clever fabrication of the nanostrings and sample mounting. The ultimate scheme to eliminate clamping loss would be to design clamping points with complete phononic bandgaps at the frequencies of the mechanical modes of the nanostrings. This was recently accomplished for very high frequency modes (> 3 GHz) [28, 29], although it is not obvious how to design such a structure for MHz frequencies and the mode shapes of nanostrings.

In conclusion, we have fabricated high Q silicon nitride nanostrings that enable multimode thermomechanical calibration. One set of devices fall upon a single curve of peak displacement versus frequency, even though the mechanical Q of these devices do not. Modes of different mode number on different strings, with identical frequency and identical peak displacement but different Q s, eliminates the possibility of bending and intrinsic loss mechanisms as dominant. Instead, clamping loss mechanisms dominate in high stress nanostrings. Engineering of the clamping dissipation promises to increase further the possible applications of nanostrings.

This work was supported by the University of Alberta, Faculty of Science; the Canada Foundation for Innovation; and the Natural Sciences and Engineering Research Council, Canada. We

thank Don Mullin, Greg Popowich and Tony Walford for technical assistance.

- [1] S.S. Verbridge, J.M. Parpia, R.B. Reichenbach, L.M. Bellan and H.G. Craighead, *J. Appl. Phys.* **99**, 124304 (2006).
- [2] S.S. Verbridge, H.G. Craighead and J.M. Parpia, *Appl. Phys. Lett.* **92**, 013112 (2008).
- [3] S. Schmid, K.D. Jensen, K.H. Nielsen and A. Boisen, *Phys. Rev. B* **84**, 165307 (2011).
- [4] Q.P. Unterreithmeier, E.M. Weig and J.P. Kotthaus, *Nature* **458**, 1001 (2009).
- [5] S. Schmid, S. Dohn and A. Boisen, *Sensors* **10**, 8092 (2010).
- [6] T. Larsen, S. Schmid, L. Grönberg, A.O. Niskanen, J. Hassel, S. Dohn and A. Boisen, *Appl. Phys. Lett* **98**, 121901 (2011).
- [7] M. Eichenfield, R. Camacho, J. Chan, K.J. Vahala and Oskar Painter, *Nature* **459**, 550 (2009).
- [8] G. Anetsberger, O. Arcizet, Q.P. Unterreithmeier, R. Rivière, A. Schliesser, E.M. Weig, J.P. Kotthaus and T.J. Kippenberg, *Nature Phys.* **5**, 909 (2009).
- [9] K.Y. Fong, W.H.P. Pernice, M. Li and H. X. Tang, *Appl. Phys. Lett* **97**, 073112 (2010).
- [10] J.D. Teufel, T. Donner, M.A. Castellanos-Beltran, J.W. Harlow and K.W. Lehnert, *Nature Nano.* **4**, 820 (2009).
- [11] K.L. Ekinci and M.L. Roukes, *Rev. Sci. Instrum.* **76**, 061101 (2005).
- [12] S.S. Verbridge, D.F. Shapiro, H.G. Craighead and J.M. Parpia, *Nano Lett.* **7**, 1728 (2007).
- [13] S.S. Verbridge, R. Ilic H.G. Craighead and J.M. Parpia, *Appl. Phys. Lett* **93**, 013101 (2008).
- [14] Q.P. Unterreithmeier, T. Faust and J.P. Kotthaus, *Phys. Rev. Lett.* **105**, 027205 (2011).
- [15] A.N. Cleland and M.L. Roukes, *J. Appl. Phys.* **92**, 2758 (2002).
- [16] D.R. Southworth, R.A. Barton, S.S. Verbridge, B. Ilic, A.D. Fefferman, H.G. Craighead and J.M. Parpia, *Phys. Rev. Lett.* **102**, 225503 (2009).
- [17] S. Schmid and C. Hierold, *J. Appl. Phys.* **104**, 093516 (2008).
- [18] J. Sulkkö, M.A. Sillanpää, P. Hakkinen, L. Lechner, M. Helle, A. Fefferman, J.M. Parpia and P.J. Hakonen, *Nano Lett.* **10**, 4884 (2010).
- [19] X.M.H. Huang, M. Manolidis, S.C. Jun and J. Hone, *Appl. Phys. Lett* **86**, 143104 (2005).
- [20] A.K. Naik, M.S. Hanay, W.K. Hiebert, X.L. Feng and M. L. Roukes, *Nature Nano.* **4**, 445 (2009).
- [21] S. Dohn, W. Svendsen, A. Boisen, and O. Hansen, *Rev. Sci. Instrum.* **78**, 103303 (2007).
- [22] J.L. Hutter and J. Bechhoefer, *Rev. Sci. Instrum.* **64**, 1868 (1993).

- [23] See supplementary material in appendix A.
- [24] J.P. Davis, D. Vick, D.C. Fortin, J.A.J. Burgess, W.K. Hiebert and M.R. Freeman, *Appl. Phys. Lett.* **96**, 072513 (2010).
- [25] W.A.P. Claassen, W.G.J.N. Valkenburg, M.F.C. Willemsen and W.M.v.d. Wijgert, *J. Electrochem. Soc.* **132**, 893 (1985).
- [26] P. Mohanty, D. A. Harrington, K. L. Ekinici, Y. T. Yang, M. J. Murphy and M. L. Roukes, *Phys. Rev. B* **66**, 085416 (2002).
- [27] G.D. Cole, I. Wilson-Rae, K. Werbach, M.R. Vanner and M. Aspelmeyer, *Nature Comm.* **2**, 231 (2011).
- [28] T.P.M., Alegre, A.H. Safavi-Naeini, M. Winger, and O. Painter, *Opt. Express* **19**, 5658 (2011).
- [29] J. Chan, T.P.M. Alegre, A.H. Safavi-Naeini, J.T. Hill, A. Krause, S. Gröblacher, M. Aspelmeyer and O. Painter, *Nature* **478**, 89 (2011).

Appendix A: Supplementary Information

The string under consideration has a uniform (volumetric) mass density ρ and a uniform cross-sectional area A . Even at rest and unstretched, the string feels a tension σA along its length because of a stress σ that is intrinsic to the material.

Any smooth string profile $z(x)$ between $x = 0$ and $x = L$ traces out a total length

$$\begin{aligned} \int_0^L \sqrt{dx^2 + dz^2} &= \int_0^L dx \sqrt{1 + (dz/dx)^2} \\ &= L + \int_0^L dx \left[\frac{1}{2}(\partial_x z)^2 - \frac{1}{8}(\partial_x z)^4 + \dots \right]. \end{aligned}$$

The string acquires excess potential energy whenever it is stretched beyond its natural length L . For small amplitude oscillations, and in the absence of any explicit dissipation mechanism, the energy stored in the string is

$$H = \int_0^L dx \left[\frac{1}{2\rho A} \Pi^2 + \frac{A\sigma}{2} (\partial_x z)^2 \right].$$

Here $\Pi(x)$ is the momentum conjugate to the displacement field. The relevant boundary conditions are $z(0) = z(L) = 0$. In the high-stress limit, the endpoints are not effectively clamped, so the gradients $z_x(0)$ and $z_x(L)$ are unrestricted.

Variation of the Hamiltonian by way of the identity

$$\frac{\delta}{\delta z(x')} (\partial_x z(x))^2 = -2\delta(x - x') \partial_x^2 z(x)$$

leads to equations of motion

$$\begin{aligned} \frac{\delta H}{\delta \Pi(x)} &= \frac{1}{\rho A} \Pi(x) = \dot{z}(x), \\ -\frac{\delta H}{\delta z(x)} &= A\sigma \partial_x^2 z(x) = \dot{\Pi}(x) = \rho A \ddot{z}(x). \end{aligned}$$

In other words, the string obeys $\sigma \partial_x^2 z = \rho \ddot{z}$. Written in terms of the normal modes,

$$z(x, t) = \sum_{n=1}^{\infty} a_n(t) \sin \frac{n\pi x}{L},$$

the continuum wave equation reduces to a discrete (but infinite: $n = 1, 2, \dots$) set of ordinary differential equations

$$\ddot{a}_n + \frac{\sigma n^2 \pi^2}{\rho L^2} a_n = \ddot{a}_n + \omega_n^2 a_n = 0.$$

Each normal modes is wholly independent and executes harmonic motion with angular frequency $\omega_n = (\sigma/\rho)^{1/2} n\pi/L$.

We proceed under the assumption that there are processes that allow energy to be shared between all the modes (ergodicity). Then, if the string is held in thermal equilibrium at temperature $T = 1/k_B\beta$, its properties are described by a partition function

$$\begin{aligned} Z &= \int \mathcal{D}[z(x)] \mathcal{D}[\Pi(x)] e^{-\beta H} \\ &= \int \mathcal{D}[z(x)] e^{-\frac{\beta A \sigma}{2} \int_0^L dx (\partial_x z)^2} \int \mathcal{D}[\Pi(x)] e^{-\frac{\beta}{2\rho A} \int_0^L dx \Pi^2}, \end{aligned}$$

which takes the form of a Boltzmann-weighted integration over the complete phase space of string shapes and momenta. The $\Pi(x)$ contribution will not enter so long as we only measure functions of the string displacement. For example,

$$\langle z(x)^2 \rangle = \frac{\int \mathcal{D}[z(x)] z(x)^2 e^{-\frac{\beta A \sigma}{2} \int_0^L dx (\partial_x z)^2}}{\int \mathcal{D}[z(x)] e^{-\frac{\beta A \sigma}{2} \int_0^L dx (\partial_x z)^2}}.$$

Once again, we want to decompose the field into its normal modes. This requires a formal change of variables in the partition function. We imagine imposing a resolution limit by breaking up the spatial domain into bins of width $\Delta x = L/N$. At each position $x_j^* = (j - \frac{1}{2})\Delta x$, the

displacement field takes a value coarse-grained $z(x_j^*) \equiv z_j = \sum_{n=1}^N a_n \sin n\pi x_j^*/L$. The infinitesimals

$$dz_j = \sum_{n=1}^N \sin \frac{n\pi(j - \frac{1}{2})}{N} da_n \equiv \sum_{n=1}^N J_{j,n} da_n$$

are connected by a matrix J that itself has no dependence on $\{z_j\}$ or $\{a_n\}$. Hence, the Jacobian of the transformation

$$\mathcal{D}[z(x)] = |\det J| \prod_{n=1}^N da_n$$

yields only an inert constant that factors out of any expectation values.

Substituting the normal mode expression into the potential energy term gives

$$\begin{aligned} \int_0^L dx \frac{A\sigma}{2} (\partial_x z)^2 &= \frac{A\sigma}{2} \int_0^L dx \left[\partial_x \sum_n a_n \sin \frac{n\pi x}{L} \right]^2 \\ &= \frac{A\rho}{4} \sum_n \omega_n^2 a_n^2 = \frac{m}{4L} \sum_n \omega_n^2 a_n^2. \end{aligned}$$

Here, we've taken advantage of the orthogonality relation

$$\int_0^L dx \cos \frac{n\pi x}{L} \cos \frac{m\pi x}{L} = \frac{L}{2} \delta_{n,m}.$$

Gaussian integration of the mode variables gives

$$\langle a_n a_m \rangle = \frac{\int [\prod_{n'} a_{n'}] a_n a_m e^{-\frac{\beta m}{4L} \sum_n \omega_n^2 a_n^2}}{\int [\prod_{n'} a_{n'}] e^{-\frac{\beta m}{4L} \sum_n \omega_n^2 a_n^2}} = \frac{2\delta_{n,m}}{\beta m \omega_n^2},$$

which confirms that the thermally averaged potential energy

$$\left\langle \int_0^L dx \frac{A\sigma}{2} (\partial_x z)^2 \right\rangle = \frac{N k_B T}{2}$$

has $k_B T/2$ per mode.

There's an important subtlety here: the expectation value $\langle a_n^2 \rangle = \frac{2k_B T}{m\omega_n^2}$ seems to imply that $\frac{1}{2}\omega_n^2 \langle a_n^2 \rangle = k_B T$ is the potential energy in the n^{th} oscillator. It is easier to make the connection with the conventional invocation of the equipartition theorem (*half* $k_B T$ per degree of freedom) if we write

$$\frac{1}{2} \frac{m}{L} \omega_n^2 \langle a_n^2 \rangle = \frac{1}{2} \tilde{\rho} \omega_n^2 \langle \alpha_n^2 \rangle = \frac{1}{2} k_B T$$

in terms of the properly normalized mode amplitude $\alpha_n = (2/L)^{1/2} a_n$ (with awkward units of distance to the half power). Here, $\tilde{\rho} = m/L$ is the linear mass density.

The average squared displacement of the thermally agitated string is

$$\begin{aligned}\langle z(x)^2 \rangle &= \sum_{n,m} \sin \frac{n\pi x}{L} \sin \frac{m\pi x}{L} \langle a_n a_m \rangle \\ &= \sum_n \frac{2k_B T}{m\omega_n^2} \sin^2 \frac{n\pi x}{L}.\end{aligned}$$

Since the spectrum is harmonic ($\omega_n = n\omega_1$), it is straightforward to evaluate this expression at the center of the string:

$$\begin{aligned}\langle z(L/2)^2 \rangle &= \frac{2k_B T}{m\omega_1^2} \sum_{\text{odd } n} \frac{1}{n^2} \\ &= \frac{2k_B T}{\rho L} \frac{\rho L^2}{\sigma \pi^2} \times \frac{\pi^2}{8} \\ &= \frac{k_B T L}{4\sigma}.\end{aligned}$$

We are interested, however, in resolving the motion in the frequency domain. To do this, we formally identify the thermal and time averaged values $\langle a_n^2 \rangle_{\text{therm}} = \langle a_n^2 \rangle_{\text{time}}$ and make use of Parseval's theorem to convert to Fourier space, treating the previous result as sum rule on the total square-displacement spectral density:

$$\langle a_n^2 \rangle = \frac{1}{t_0} \int_0^{t_0} dt |a_n(t)|^2 = \int_0^\infty d\omega S_n(\omega) = \frac{2k_B T}{m\omega_n^2}.$$

For the undamped oscillator case we have considered so far,

$$S_n(\omega) = \frac{2k_B T}{m\omega_n^2} \delta(\omega - \omega_n),$$

but we expect the peak to be broadened once dissipation is introduced. We can solve the relevant damped harmonic oscillator

$$\ddot{a}_n + \frac{\omega_n}{Q_n} \dot{a}_n + \omega_n^2 a_n = \frac{f(t)}{m}$$

[appearing as Eq. (2)] by applying the usual trick of driving it at a single frequency and complexifying the variable $a_n(t) = \text{Re } \tilde{a}_n e^{i\omega t}$. From

$$(-\omega^2 + i\omega \frac{\omega_n}{Q_n} + \omega_n^2) \tilde{a}_n = \frac{f(\omega)}{m} = C$$

we get

$$a_n = \frac{C \sin(\omega_n t + \phi_n)}{\sqrt{(\omega_n^2 - \omega^2)^2 + (\omega \omega_n / Q_n)^2}}$$

with a phase shift $\phi_n = \arctan[2\omega\omega_n Q_n^{-1}/(\omega^2 - \omega_n^2)]$. The unknown C is constant (independent of ω) because the thermal noise is white. Its value can be fixed by taking the time-averaged square displacement

$$\langle a_n \rangle^2 = \frac{\frac{1}{2}C^2}{(\omega_n^2 - \omega^2)^2 + (\omega\omega_n/Q_n)^2}$$

and equating the integral

$$\int_0^\infty d\omega \frac{\frac{1}{2}C^2}{(\omega_n^2 - \omega^2)^2 + (\omega\omega_n/Q_n)^2} = \frac{1}{2}C^2 \frac{\pi Q_n}{2\omega_n^3}$$

with the known weight under the curve, $2k_B T/m\omega_n^2$. This establishes that

$$\frac{1}{2}C^2 = \frac{4k_B T}{m\pi Q_n}$$

and in turn yields

$$S_n(\omega) = \frac{4\omega_n k_B T}{m\pi Q_n [(\omega_n^2 - \omega^2)^2 + (\omega\omega_n/Q_n)^2]}.$$

The corresponding expression in terms of conventional frequency is

$$S_n(\nu) = 2\pi S_n(\omega) = \frac{\nu_n k_B T}{m\pi^3 Q_n [(\nu_n^2 - \nu^2)^2 + (\nu\nu_n/Q_n)^2]}.$$

At the peak of the distribution

$$\nu_n^{\max} = \nu_n \sqrt{1 - \frac{1}{2Q_n^2}}$$

the value is

$$S_n(\nu_n^{\max}) = \frac{Q_n k_B T}{m\pi^3 (1 - \frac{1}{4Q_n^2}) \nu_n^3}.$$

In the experimental situation, the relevant quantity is the power spectral density, obtained by squaring the measured voltage near resonance by the bandwidth of the lock-in amplifier. It is related to the square-displacement spectral density by

$$\begin{aligned} S_V &= \frac{V^2}{\Delta\nu} = (\text{noise floor}) + \alpha S_z(\nu) \\ &= s_0 + \left(\frac{\alpha k_B T}{m\pi^3} \right) \frac{\nu_n}{Q_n [(\nu_n^2 - \nu^2)^2 + (\nu\nu_n/Q_n)^2]}, \end{aligned}$$

where α is a conversion factor having units V^2/m^2 . It is straightforward to extract α and s_0 from a fit to the data. (There is a unique α associated with each peak.) Hence, from the measured voltage we report a root square-displacement spectral density according to

$$\sqrt{S_z(\nu)} = \frac{V}{\sqrt{\alpha \Delta\nu}}.$$